
CATALYSIS IN CHEMICAL
AND PETROCHEMICAL INDUSTRY

Study of Carbon Dioxide Hydrogenation to Hydrocarbons Over Iron-Based Catalysts: Synergistic Effect¹

Isa Shahroudbari^{a, *}, Yaghoob Sarrafi^{a, **}, and Yahya Zamani^{b, ***}

^a Faculty of Chemistry, University of Mazandaran, Mazandaran, 13534-47416 Iran

^b Gas Research Division, Research Institute of Petroleum Industry, West Blvd. of Azadi Sport Complex, Tehran, 14857-33111 Iran

*e-mail: isa.shahroudbari@stu.umz.ac.ir

**e-mail: ysarrafi@umz.ac.ir

***e-mail: yahyazamani@yahoo.com

Received January 26, 2021; revised April 6, 2021; accepted April 8, 2021

Abstract—Hydrogenation of CO₂ to CO and hydrocarbons is carried out over a wide range of catalysts. Group of VIII B transition metals have proved high conversion and selectivity for CO and methane. Meanwhile, low cost and effective catalysts are preferable in an industrial scale. In this work, the synergistic effect of iron content on the catalytic performance were investigated in carbon dioxide hydrogenation reaction. Incipient wetness impregnation procedure was used for the preparation of four γ-Al₂O₃ supported iron-based catalysts. BET, XRD, H₂-TPR and TEM techniques were employed for the catalyst characterization. The evaluation of catalysts were carried out in a fixed bed reactor at the process conditions of temperature of 300°C, pressure of 20 atm, H₂ to CO₂ ratio of 3 and GHSV of 3 NL/(h g_{Cat}). It was found that the promoter addition improves the activity of Fe catalyst for both Fischer-Tropsch synthesis (FTS) and Reverse Water Gas Shift (RWGS) reactions. The results showed that conversion of CO₂ was from 15.6 to 35.6% with major products of methane, C₂ to C₄, C₅+ and CO. It was also found that impact of K and Ce promoters into iron catalyst showed the highest conversion and hydrocarbon yield due to the synergistic effect.

Keywords: iron catalyst, promoters, characterization, CO₂ hydrogenation, synergistic effect

DOI: 10.1134/S2070050421040085

1. INTRODUCTION

The problem of global warming is related to increasing of CO₂ emissions. CO₂ is not only one of the main greenhouse gases that is caused global warming but it also is an inexpensive, abundant and readily available chemical [1–4]. Hydrogenation of carbon dioxide to methanol is a solution to solve two main problems needed to reduce CO₂ emissions and the reduction in the usage of fossil fuels. As an ideal strategy for the use of CO₂, hydrogenation of CO₂ and the production of chemicals and fuels such as methane, methanol, syngas and dimethyl ether have been already considered [5–8]. One of the best ways to reduce environmental degradation and future shortages of fossil fuels production of hydrocarbons is through hydrogenation of CO₂ within the modification of Fischer-Tropsch Synthesis (FTS), which CO₂ is used instead of CO.

The structure of the catalyst for CO₂ hydrogenation is similar to that of FTS. Hydrogenation of CO₂ is a

sequential reaction to reduce CO₂ to CO and then CO hydrogenation for producing various hydrocarbons compounds and oxygenated compounds [9, 10]. The distribution of the hydrocarbon products due to the hydrogenation of carbon dioxide is similar to the hydrogenation of carbon monoxide at the same temperature and pressure conditions [11]. Investigation of this subject have been done, which can be divided into two categories: methanol-mediated and non-methanol-mediated reactions [12, 13]. In the methanol intermediate method, CO₂ and H₂ react in the presence of copper-zinc catalysts to produce methanol, which is subsequently converted to other hydrocarbons such as gasoline [14]. In the second one, CO₂ hydrogenation occurs through two steps: Reverse Water Gas Shift (RWGS) reaction and FT synthesis. Iron oxides are used as catalysts in the FT process, which is active in both Water Gas Shift (WGS) and RWGS reactions [15, 16]. Iron catalysts are attractive for the synthesis of hydrocarbons due to the production of olefinic products [17]. One method of converting CO₂ to liquid fuels is to hydrogenate CO₂ through modified Fisher-Tropsch synthesis in the presence of

¹ The paper is published in the original.

catalysts. Riedel et al. investigated the catalytic performance of Fe and Co catalysts in the mixtures of CO, CO₂ and H₂. As CO₂ increases and CO in the feed (syngas) decreases, the composition of the products obtained from the Co catalysts changes from heavy hydrocarbons to almost methane, while iron catalysts result in the same hydrocarbon products as CO₂/H₂ or CO/H₂ [18]. It has been found that iron catalysts containing various promoters such as potassium, copper and manganese improved its performance [19]. In this paper, the hydrogenation of carbon dioxide were investigated in four iron-based catalysts. Moreover, the synergistic effects between the promoters were studied for this reaction. The catalysts were characterized using different techniques of BET, XRD, H₂-TPR and TEM.

2. EXPERIMENTAL

2.1. Catalyst Preparation

The Fe catalysts were synthesized via wet impregnation method. In this procedure, an aqueous solution of Fe(NO₃)₃·9H₂O (Aldrich, 99.99%), Cu(NO₃)₂·4H₂O (Alfa Aesar, ≥98%) and Zn(NO₃)₂·4H₂O (98.5%), KNO₃ (Aldrich, 99.0%) or Ce(NO₃)₃·4H₂O (Aldrich, ≥99.99%) or both of K/Ce salts [20] was prepared. γ-Al₂O₃ support (Condea Vista Catalox B γ-alumina) is used as a powder form. Typically, 7 g of γ-Al₂O₃ support was impregnated with 16 mL of the solution. The impregnated sample was dried at 120°C for 24 h in an electric oven, then samples were calcinated in a furnace at 400°C for 3 h. The catalyst compositions were designated in terms of the weight ratios as 15Fe/γ-Al₂O₃; 15Fe/3Cu/10Zn/2K/γ-Al₂O₃; 15Fe/3Cu/10Zn/2Ce/γ-Al₂O₃, and 15Fe/3Cu/10Zn/1K/1Ce/γ-Al₂O₃. All catalysts were pressed into pellets, crushed, and sieved to obtain particle sizes in the range of 20–30 mesh.

2.2. Catalyst Characterization

BET Surface area, pore volume and mean pore size of the catalysts were determined in a Micromeritics Tri star 3020 automated system. An XRD spectrum of fresh catalysts were conducted with a Philips PW1840 X-ray diffractometer with monochromatized CuK_α radiation to determine the catalysts phases. Temperature—Programmed Reduction (TPR) profile of the calcined catalysts were recorded using a Micromeritics TPD-TPR 2900 system. The TPR of 50 mg of each sample was performed in 5% H₂–95% Ar gas mixture. The catalysts were heated from 50 to 900°C at 10°C/min. Average particle size of the calcined catalysts were investigated by LEO 912AB Transmission Electron Microscopy (TEM).

2.3. Catalytic Activity Test

As shown in Fig. 1, the catalytic reaction was conducted in a fixed-bed stainless steel reactor. Electronic mass flow and pressure controllers are used to control the flow rate of feed and the pressure of reactor. The required amount of catalyst (2 g) was conducted into a stainless steel reactor with inner diameter of 0.95 cm and length of 70 cm. The length of catalyst bed in every loading is about 9 cm [21, 22]. The catalyst was reduced by a 20% H₂–80% N₂ flow gas at 400°C for 2 h. After the activation process, CO₂ hydrogenation was carried out under the operational conditions of pressure of 20 atm, temperature of 300°C, H₂/CO₂ ratio of 3, GHSV of 3 NL/(h g_{Cat}). The products were analyzed online by a gas chromatography (GC) of Agilent 7890A [19, 20]. Using GC analysis, CO₂ conversion and product selectivity were calculated and the following equations were used (Eqs. (1)–(5)):

$$n_{\text{products}} = \text{moles CO}_{\text{out}} + \sum_{i=1}^n i \quad (1)$$

× moles of hydrocarbon_{*i*},
i = atomic number of carbon,

$$\text{selectivity of CO (\%)} = \frac{\text{moles CO}_{\text{out}} \times 100}{n_{\text{products}}}, \quad (2)$$

$$\begin{aligned} & \text{Selectivity of hydrocarbon (\%)} \\ & = \frac{\sum_{i=1}^n i \times \text{moles of hydrocarbon}_i \times 100}{n_{\text{products}}}, \quad (3) \end{aligned}$$

$$\begin{aligned} & \text{Hydrocarbon distribution (\%)} \\ & = \frac{i \times \text{moles of hydrocarbon}_i \times 100}{\sum_{i=1}^n i \times \text{moles of hydrocarbon}_i}, \quad (4) \end{aligned}$$

$$\text{CO}_2 \text{ conversion} = \frac{(F_{\text{CO}_2, \text{in}} - F_{\text{CO}_2, \text{out}})}{F_{\text{CO}_2, \text{in}}} \times 100. \quad (5)$$

3. RESULTS AND DISCUSSION

3.1. Catalyst Characterization Results

Surface area, pore volume and mean pore size of the prepared catalysts were measured using a BET instrument. An appropriate amount of catalyst (0.3 g) was taken into the sample tube and slowly heated to 300°C for 2 h. The sample was then transferred to the adsorption unit, and the N₂ adsorption/desorption was measured. The results obtained from BET for prepared catalysts are illustrated in Table 1. According to the BET results:

By adding Fe, Cu, Zn, K and Ce to the support, the BET surface area and pore volume were decreased. Furthermore, it might promote the aggregation of the

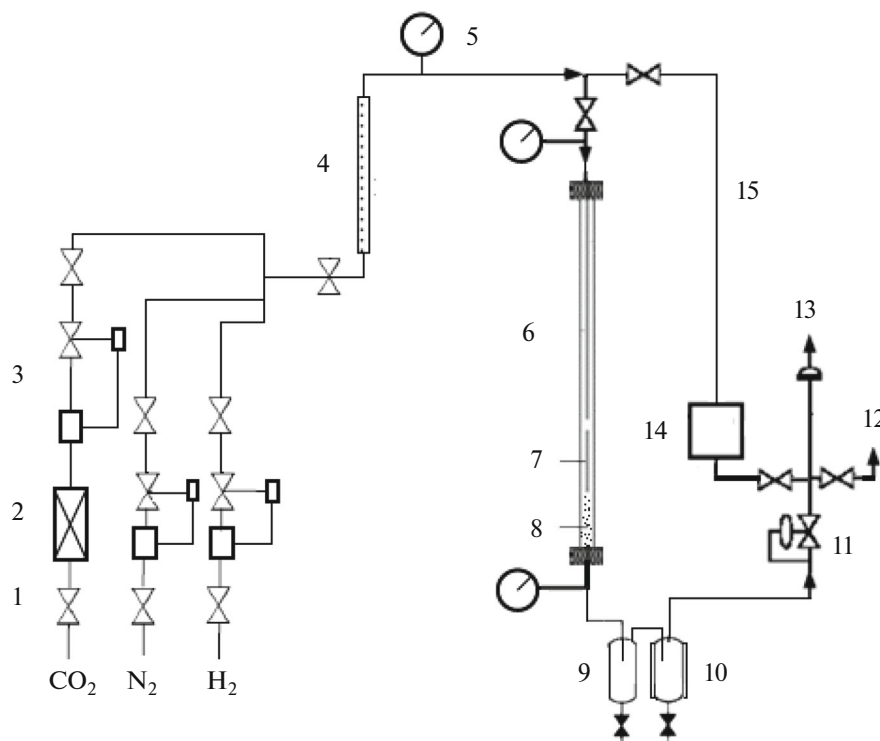


Fig. 1. The schematic diagram of fixed-bed reactor system: (1) valve; (2) carbonyl trap; (3) mass flow controller; (4) static mixer; (5) pressure gauge; (6) fixed-bed reactor; (7) catalyst; (8) quartz; (9) hot trap; (10) cold trap; (11) back pressure regulator; (12) wet gas flow meter; (13) vent; (14) gas chromatography; (15) by-pass line.

catalyst crystallites and block up the pores. Figure 2 shows the XRD patterns for the three catalysts and $\gamma\text{-Al}_2\text{O}_3$ support. The patterns of the catalysts show the peaks at $2\theta = 37.6^\circ$, 39.5° , 45.8° , and 66.8° attributed to the primary support of $\gamma\text{-Al}_2\text{O}_3$ support. For the three calcined iron catalysts, in addition to the peaks attributed to the $\gamma\text{-Al}_2\text{O}_3$ support, the peaks of hematite, Fe_2O_3 at 24.1° , 33.3° , 35.7° , 41° , 49.5° , 54.2° , 62.3° , and 64.2° can be intuited. In the XRD pattern associated with the magnetite phase, exist two additional peaks located at 24° and 26.10° . On the other hand, the formation of FeAl_2O_4 spinel cannot be discarded. The diffraction peaks corresponding to the

second metal oxide phases were not observed in the calcined catalysts [23].

TEM image revealed the morphology of the catalyst. TEM images of $\text{Fe-Zn-Cu (K-Ce)/}\gamma\text{-Al}_2\text{O}_3$ catalysts are presented in Fig. 3. Irregular shapes and agglomerated particles with the size of 20–80 nm are shown for the catalysts. The elements of Fe-Zn-Cu with combination of Ce and K are well dispersed over the surface of $\gamma\text{-Al}_2\text{O}_3$. Catalyst morphology was rough as all the particles were aggregated and agglomerated over the surface of the support [24, 25].

$\text{H}_2\text{-TPR}$ determines the reduction behavior of the catalysts. The first peak is the transformations of CuO to Cu

Table 1. Surface area, pore volume and mean pore diameter of the catalysts

Catalysts	BET, m^2/g	Pore volume, cm^3/g	Average pore diameter, nm
$\gamma\text{-Al}_2\text{O}_3$ Support	209.52	0.69	12.73
$\text{F}^*/\gamma\text{-Al}_2\text{O}_3$	168.52	0.44	11.21
$\text{FCZ}^{**}/2\text{K}/\gamma\text{-Al}_2\text{O}_3$	123.71	0.30	9.65
$\text{FCZ}/2\text{Ce}/\gamma\text{-Al}_2\text{O}_3$	129.54	0.37	10.25
$\text{FCZ}/1\text{K}/1\text{Ce}/\gamma\text{-Al}_2\text{O}_3$	134.63	0.38	10.78

* F = 15Fe.

** FCZ = 15Fe/3Cu/10Zn.

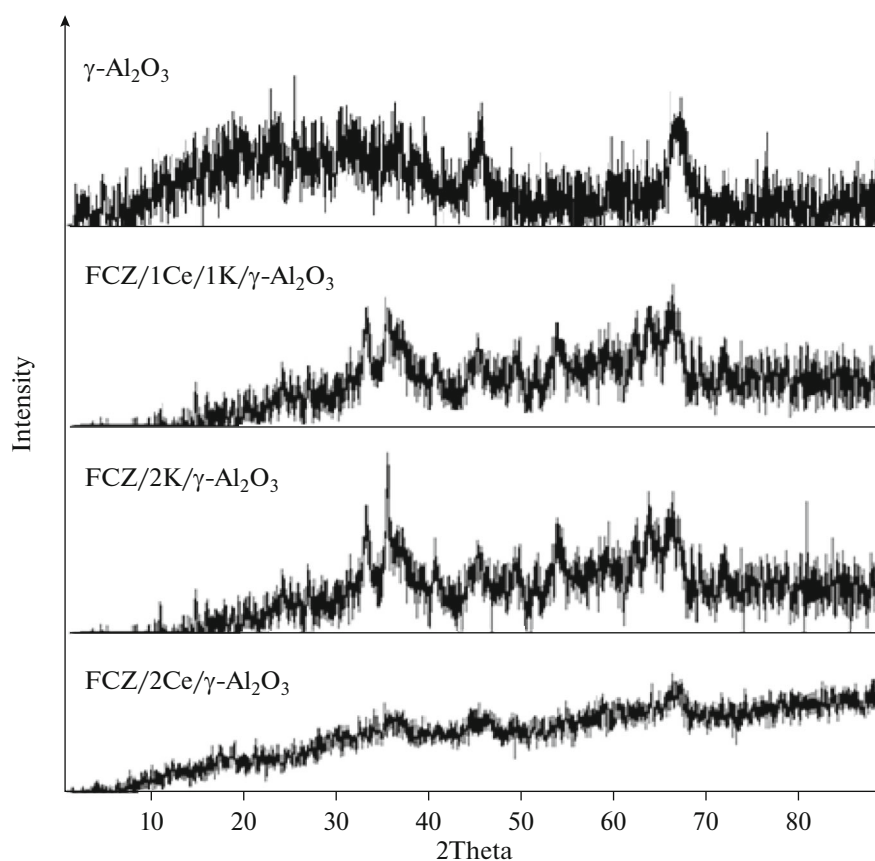


Fig. 2. X-ray diffraction patterns of the catalysts.

(1) $\text{CuO} \rightarrow \text{Cu}$.

The second peak is the transformation of Fe_2O_3 to Fe_3O_4 , and the third peak represents the transformation of Fe_3O_4 to Fe [20, 23]

(2) $\text{Fe}_2\text{O}_3 \rightarrow \text{Fe}_3\text{O}_4$,

(3) $\text{Fe}_3\text{O}_4 \rightarrow \text{Fe}$.

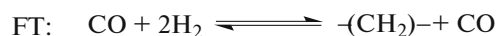
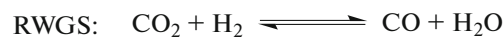
Hydrogen consumption occurs mainly at 160–420°C due to the simultaneous reduction of CuO to Cu and Fe_2O_3 to Fe_3O_4 . The reduction of iron catalysts by hydrogen is known to be a two or three-staged process [26–29]. In this process, Fe_2O_3 is first reduced at 397°C to Fe_3O_4 , which is reduced to metallic iron at 690°C [28]. In all catalysts, iron oxides were reduced to Fe_3O_4 and they are probably converted partly to oxygen-deficient Fe_3O_4 species during the TPR to 400°C. H_2 -TPR profile of the catalysts are shown in Fig. 4.

According to Fig. 4, the un-promoted iron catalyst (F) exhibited two peaks attributed to the reduction by H_2 at around 340 and 620°C, which corresponds to the two-step reduction of hematite (reactions (2) and (3)) [30–32]. Each catalysts of FCZ2K, FCZ2Ce and FCZ1K1Ce exhibited three peaks attributed to the reduction at around (220, 330 and 630°C), (230, 340

and 590°C) and (210, 315, 530°C), respectively, which correspond to the three-step reduction (reactions of 1, 2 and 3). The reduction of Fe species can be promoted by the addition of Cu species, leading to a shift of a peak attributed to the reduction of Fe_2O_3 to Fe_3O_4 to a lower temperature in H_2 -TPR profiles [30, 31], whereas K and Ce species suppresses the reduction of Fe species due to the interaction between K species and the metal species [33]. However, the second and third peaks of all the promoted iron-based catalysts was shifted to higher temperatures in comparison with that of the FCZ1K1Ce catalyst. Iglesia and coworkers exhibited the initial removal of only a very small amount of lattice oxygen from Fe_2O_3 which facilitated the formation of the active sites during the FTS reaction [34].

3.2. CO_2 Hydrogenation Over Iron Supported $\gamma\text{-Al}_2\text{O}_3$ Catalysts

CO_2 hydrogenation is performed in two steps with the CO intermediate being formed by the reverse water–gas shift (RWGS) reaction [26]:



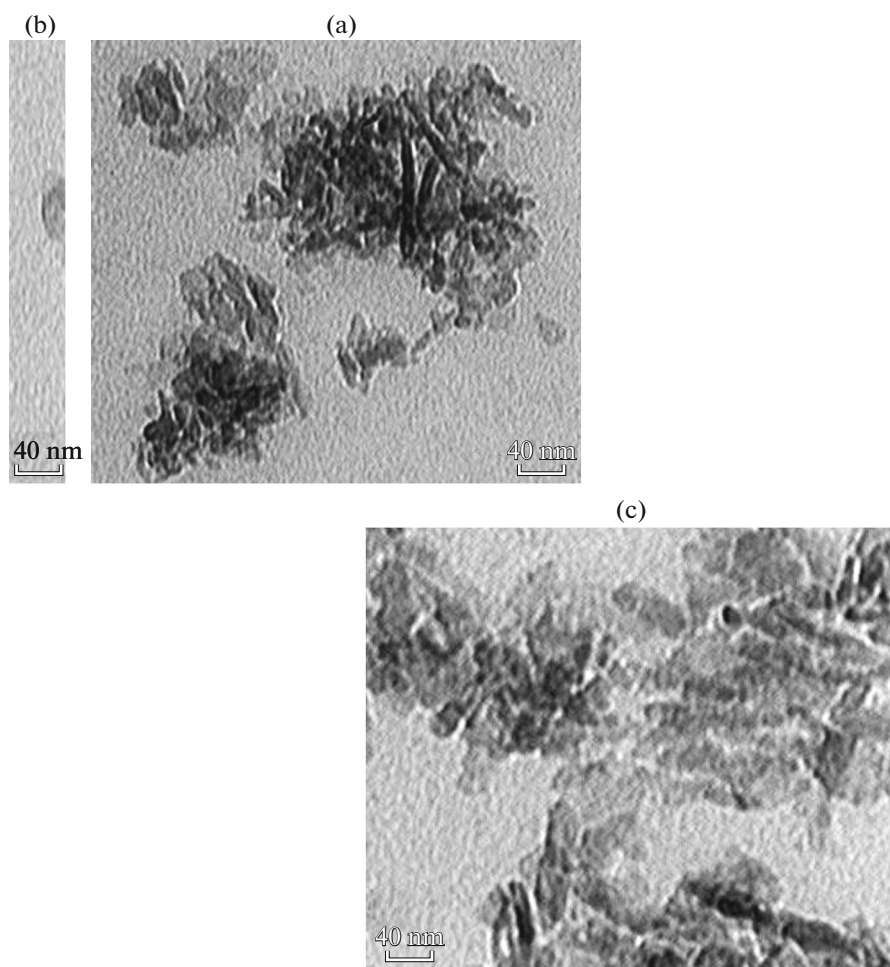


Fig. 3. TEM images of the catalysts. (a)FCZ/2K/ γ -Al₂O₃ (b) FCZ/2Ce/ γ -Al₂O₃ (C) FCZ/1K/1Ce/ γ -Al₂O₃.

CO₂ conversion and product selectivity were calculated using the data collected at 32 h time on stream. Products selectivity of the catalysts are indicated in Table 2. It shows that promoters affect on the selectivity of light hydrocarbons (methane and C₂–C₄), and heavy hydrocarbons (C₅⁺). Based on the above discussion, the catalytic performances of CO₂ hydrogenation over different catalysts are compared and listed in Table 2.

The product distribution (C₅⁺) that is represented by carbon number and Productivity ($g_{\text{Hydrocarbon}}/(h \text{ g}_{\text{Cat}})$) are shown in Fig. 5. Hydrocarbon chain is formed by step-wise insertion or addition of C₁ with constant growth probability (α), the chain length distribution can be modelled by Anderson–Schulz–Flory (ASF) distribution assuming a constant value for α :

$$\log W_n/n = n \log \alpha + \text{const.} \quad (6)$$

here W_n is the mass fraction of the species with carbon number n and α is chain growth probability. By plotting of $\log (W_n/n)$ versus n , α can be obtained from the

slope [43]. The calculated α of four types of catalysts including F/ γ -Al₂O₃; FCZ/2K/ γ -Al₂O₃; FCZ/2Ce/ γ -Al₂O₃, and FCZ/1K/1Ce/ γ -Al₂O₃ are 0.58; 0.72; 0.64; 0.68, respectively.

CO₂ hydrogenation over iron catalysts is occurred through a consecutive mechanism in which CO₂ is first converted to CO by the RWGS reaction, and then CO is hydrogenated to produce hydrocarbons. Therefore, the mechanism of hydrocarbon chain growth from carbon dioxide is similar to that of CO hydrogenation (FT process). K has been extensively studied as a promoter of iron-based FT catalysts. It has been shown that it favors CO and CO₂ adsorption and increases the production of hydrocarbons. The CO₂ conversion of catalysts at identical operating conditions was recorded for about 48 h. In Fig. 6, the CO₂ conversion of the catalysts decreases with time on stream. Promoters increase intrinsic activity of surface sites by lowering the activation energy or entropy for a chemical reaction [10].

For Ce-promoted Fe catalyst, the CO₂ conversion is reduced in different time. Moreover, addition of the

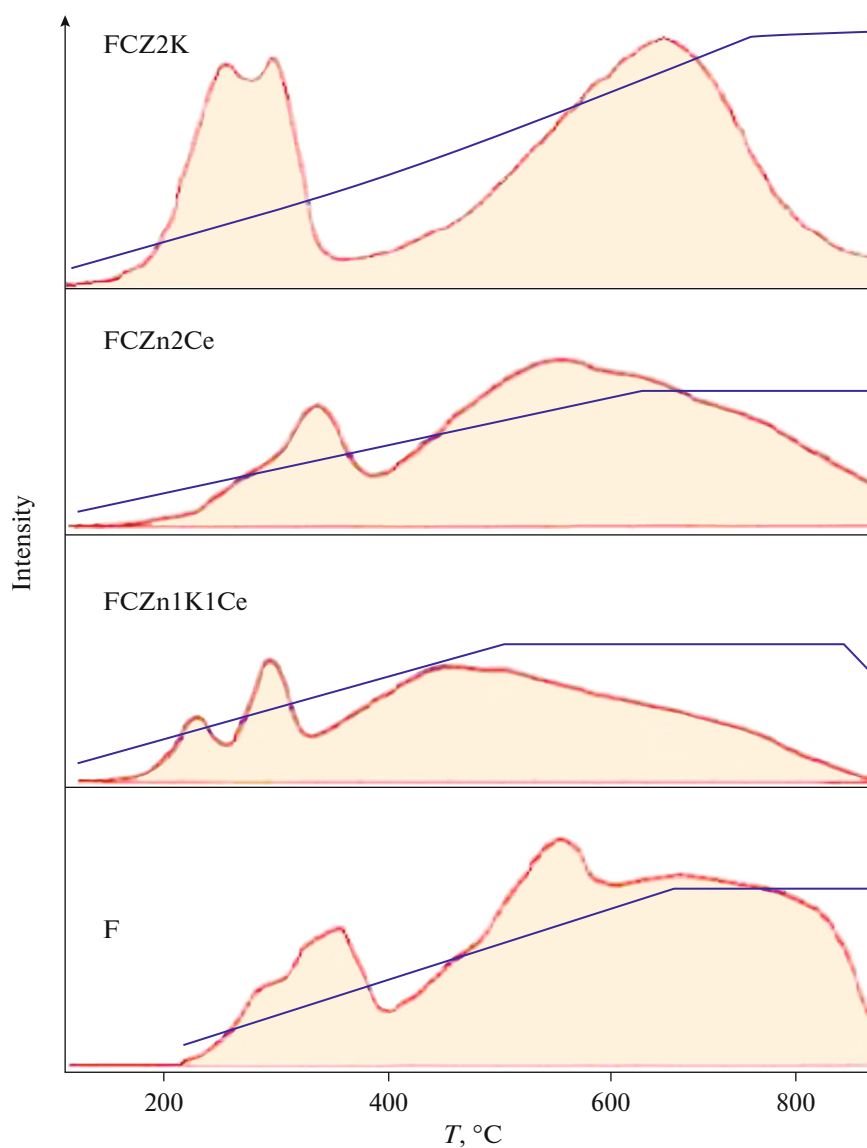


Fig. 4. H₂-TPR profile of the catalysts.

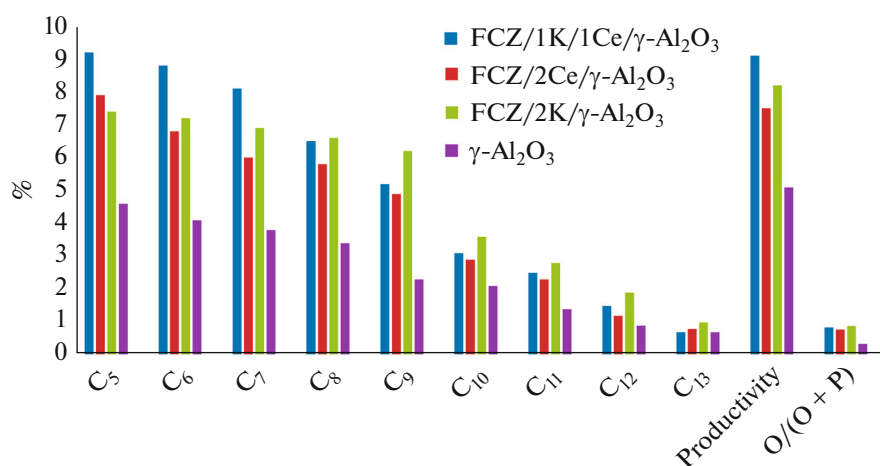


Fig. 5. C₅⁺ product distribution and productivity of the catalysts. O = Olefin; P = Paraffin; Productivity = g Hydrocarbon × 100/(h g_{Cat}).

Table 2. The activity and selectivity of the literature overview catalysts and present work

Catalysts	H ₂ /CO ₂	T, °C	P, atm	GHSV ^a	X _{CO₂}	S _{CO}	S _{C1}	S _{C2–C4}	S _{C5+}	Ref.
Fe/Al ₂ O ₃	3	300	10.1	31.6	22.8	N.G. ^b	43.2	48.08	8.8	[35]
Fe	3	300	10	22	16.6	43	43.4	51.9	4.6	[36]
Fe–Cu	3	300	10	22	10.9	59.8	55.3	42.1	2.6	[36]
Fe–Cu–K	3	300	10	22	21.8	35.7	20.7	55.5	23.8	[36, 37]
Fe–Cu/K–Al ₂ O ₃	3 ^c	340	20	75	36	10.2	17.8	50.1	2.7	[38]
Fe ₂ O ₃	3	300	25	9.3	30.8	15.7	30.1	38.4	15.8	[39]
10Fe–2.4K	3	300	25	9.3	37.8	6.0	8.3	27.8	56	[39]
Fe	3	300	11	60	19.9	23	27	29	21	[40]
Fe–Cu–K	3	300	11	60	19.9	51	12	21	16	[40]
Fe–K/Al ₂ O ₃	3	300	25	33.3	36.6	9.6	12.4	34.3	43.7	[41]
Fe–K/HPCMS-1	3	400	30	60	33.4	38.9	13.5	29.5	18.1	[42]
F ^d	3	300	20	50	15.6	10.9	44.1	21.6	23.3	T.W. ^e
FCZ/2K	3	300	20	50	27.7	8.7	32.4	15.3	43.6	T.W.
FCZ/2Ce	3	300	20	50	30.2	7.3	35.6	18.5	38.6	T.W.
Fcz/1K/1Ce	3	300	20	50	35.6	6.8	31.2	16.4	45.6	T.W.

X_{CO₂} = CO₂ Conversion (%); S_{CO} = CO selectivity; S = selectivity; ^amL/(min g_{Cat}); ^bnot given; ^cCO₂ : H₂ : N₂ = 3 : 1 : 1; ^dFe; ^ethis work.

K₂O has more destructive effect on CO₂ conversion. It illustrates the catalyst FeCuZn-1Ce-1K/γ-Al₂O₃ with highest selectivity and almost relatively high CO₂ conversion possesses highest productivity.

4. CONCLUSIONS

In this paper, iron promoted catalysts were synthesized using incipient wet impregnation method. The calcined catalysts were characterized using XRD, BET, H₂-TPR and TEM techniques. The catalysts conducted in a fixed-bed reactor. The activity of the catalysts were evaluated in CO₂ hydrogenation at pressure, temperature, H₂/CO₂ ratio and GHSV of 20 atm,

300°C, 3,3 NL/(h g_{Cat}) respectively. The catalysts were active in CO₂ hydrogenation reaction with conversions of approximately 15.6–35.6%. The RWGS reaction can be effectively catalyzed by iron-based catalysts. The addition of promoters such as K and Ce remarkably enhanced the CO₂ conversion. The promotional effect is ascribed to the strong interaction between Fe and K/Ce, altering the electronic density of iron and thus facilitating CO₂ activation on the catalytic surface. As compared with individual promoter of K or Ce, double promoters of K and Ce significantly improved CO₂ conversion and improved hydrocarbon yield, which are due to the synergistic effect of the promoters.

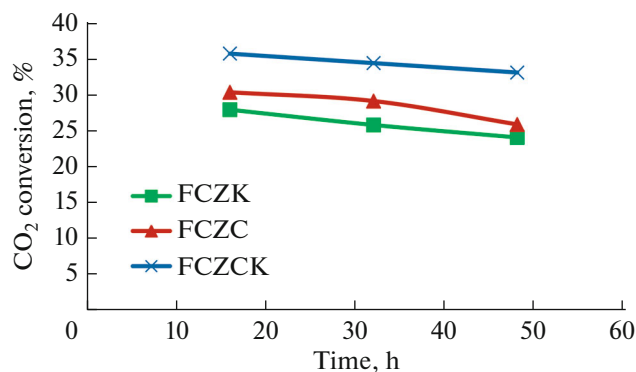


Fig. 6. CO₂ conversion trend as a function of time on stream for the catalysts.

REFERENCES

- Larcher, D. and Tarascon, J.M., *Nat. Chem.*, 2015, vol. 7, pp. 19–29.
- Lund, H., *Energy*, 2007, vol. 32, pp. 912–919.
- Edwards, P.P., Kuznetsov, V.L., David, W.I.F., and Brandon, N.P., *Energy Policy*, 2008, vol. 36, pp. 4356–4362.
- Chu, S. and Majumdar, A., *Nature*, 2012, vol. 488, pp. 294–303.
- Chuasomboon, N., Numpilai, T., and Chareonpanich, K.M., *Fuel*, 2019, vol. 241, pp. 695–703.
- Ren, S.J., Fan, X., Shang, Z.Y., Shoemaker, W.R., Ma, L., and Wu, T.P., *J. CO₂ Util.*, 2020, vol. 36, pp. 82–95.
- Li, B., Duan, Y., Luebke, D., and Morreale, B., *Appl. Energy*, 2013, vol. 102, pp. 1439–1447.

8. Frusteri, F., Bonura, G., Cannilla, C., Cordaro, M., Ferrante, D., and Aloise, A., *Appl. Catal., B*, 2015, vols. 176–177, pp. 522–531.
9. Frusteri, F., Cordaro, M., Cannilla, C., and Bonura, G., *Appl. Catal., B*, 2015, vol. 162, pp. 57–65.
10. Pijolat, M., Perrichon, V., Primet, M., and Bussi re, P., *J. Mol. Catal.*, 1982, vol. 17, pp. 367–380.
11. Schulz, H., Schaub, G., Claeys, M., and Riedel, T., *Appl. Catal., A*, 1999, vol. 186, pp. 215–227.
12. Fujimoto, K. and Shikada, T., *Appl. Catal.*, 1987, vol. 3, pp. 13–23.
13. Lee, J.F., Chern, W.S., Lee, M.D., and Dong, T.Y., *Can. J. Chem. Eng.*, 2009, vol. 70, pp. 511–515.
14. Prasad, P.S.S., Bae, J.W., Jun, K.W., and Lee, K.W., *Catal. Surv. Asia*, 2008, vol. 12, pp. 170–183.
15. Schulz, H., *Appl. Catal., A*, 1999, vol. 186, pp. 3–12.
16. Van Der Laan, G.P. and Beenackers, A.A.C.M., *Catal. Rev. Sci. Eng.*, 1999, vols. 255–318, p. 41.
17. Williams, K.J., Boffa, A.B., Salmeron, M., Bell, A.T., and Somorjai, G.A., *Catal. Lett.*, 1991, vol. 9, pp. 415–426.
18. Riedel, T., Schaub, G., Jun, K., and Lee, K., *Ind. Eng. Chem. Res.*, 2001, vol. 40, pp. 1355–1363.
19. Wang, J., You, Z., Zhang, Q., Deng, W., and Wang, Y., *Catal. Today*, 2013, vol. 215, pp. 186–193.
20. Shahroudbari, I., Sarrafi, Y., Hoseinzadeh, R., and Zamani, Y., *Pet. Coal*, 2020, vol. 62, no. 4, pp. 1572–1576.
21. Arsalanfar, M., Mirzaei, A. A., Atashi, H., Bozorgzadeh, H.R., Vahid, S., and Zare, A., *Fuel Process. Technol.*, 2012, vol. 96, pp. 150–159.
22. Mirzaei, A.A., Pourdolat, A., Arsalanfar, M., Atashi, H., and Samimi, A.R., *J. Ind. Eng. Chem.*, 2013, vol. 19, pp. 1144–1152.
23. Zamani, Y., Bakavoli, M., Rahimizadeh, M., Mohajeri, A., and Seyedi, S.M., *Chin. J. Catal.*, 2012, vol. 33, pp. 1119–1124.
24. Farias, F.E.M., Neto, R.C.R., Baldanza, M.A.S., Schmal, M., and Fernandes, F.A.N., *Braz. J. Chem. Eng.*, 2011, vol. 28, pp. 495–504.
25. S nchez De La Torre, F., Rivera De La Rosa, J., Kharisov, B.I., and Lucio-Ortiz, C.J., *Materials*, 2013, vol. 6, pp. 4324–4344.
26. Kishan, G., Lee, M.W., Nam, S.S., Choi, M.J., and Lee, K.W., *Catal. Lett.*, 1998, vol. 56, pp. 215–219.
27. Nam, S.S., Kim, H., Kishan, G., Choi, M.J., and Lee, K.W., *Appl. Catal., A*, 1999, vol. 179, pp. 155–163.
28. Riedel, T., Claeys, M., Schulz, H., Schaub, G., Nam, S.S., Jun, K.W., Choi, M.J., Kishan, G., and Lee, K.W., *Appl. Catal., A*, 1999, vol. 186, pp. 201–213.
29. Jozwiak, W.K., Goralski, J., and Domka, F., *Appl. Catal., A*, 2000, vol. 190, pp. 107–115.
30. Jin, Y. and Datye, A.K., *J. Catal.*, 2000, vol. 196, no. 1, pp. 8–17.
31. Wan, H.J., Wu, B.S., and Zhang, C.H., *Catal. Commun.*, 2007, vol. 8, no. 10, pp. 1538–1545.
32. Bukur, D.B. and Sivaraj, C., *Appl. Catal., A*, 2002, vol. 231, nos. 1–2, pp. 201–214.
33. Zhang, H., Ma, H., Zhang, H., Ying, W., and Fang, D., *Catal. Lett.*, 2012, vol. 142, no. 1, pp. 131–137.
34. Li, S., Ding, W., Meitzner, G.D., and Iglesia, E., *J. Phys. Chem. B*, 2002, vol. 106, pp. 85–91.
35. Riedel, T., Claeys, M., Schulz, H., Schaub, G., Nam, S.S., Jun, K.W., Choi, M.J., Kishan, G., and Lee, K.W., *Appl. Catal., A*, 1999, vol. 186, pp. 201–213.
36. Herranz, T., Rojas, S., P rez-Alonso, F., J., Ojeda, M., Terreros, P., and Fierro, J. L.G., *Appl. Catal., A*, 2006, vol. 311, pp. 66–75.
37. Lisheng, G., Jian, S., Qingjie, G., and Noritatsu, T., *J. Mater. Chem. A*, 2018, vol. 6, pp. 23244–23262.
38. Nawapat, C., Thanapha, N., Chin, K.C., Nuchanart, S., Thana S., Chularat W., Jumras, L., and Thongthai, W., *Fuel*, 2021, vol. 283. <https://doi.org/10.1016/j.fuel.2020.119248>
39. Jiang, F., Liu, B., Geng, S., Xu, Y., and Liu, X., *Catal. Sci. Technol.*, 2018, vol. 8, no. 16, pp. 4097–4107.
40. Zhang, A., Liu, M., Li, J., Song, F., Song, C., and Guo, X., *RSC Adv.*, 2016, vol. 2016, pp. 10831–10836.
41. Nuttakorn, B., Xiao, J., Chunshan, S., and Pattarapan, P., *Top. Catal.*, 2018, vol. 61, nos. 15–17, pp. 1–14.
42. Sun-Mi, H., Chundong, Z., Seung, J.H., Hae-Gu, P., Yong, T.K., Sunkyu, Y., Ki-Won, J., and Seok, K.K., *J. CO2 Util.*, 2020, vol. 37, pp. 65–73.
43. Patzlaff, J., Liu, Y., Graffmann, C., and Gaube, J., *Appl. Catal., A*, 1999, vol. 186, pp. 109–119.